Flight Dynamics and Control Strategy of Electric Solar Wind Sails

Gangqiang Li*, Zheng H. Zhu† and Chonggang Du‡

York University, 4700 Keele Street, Toronto, Ontario, M3J 1P3, Canada

This paper studies the flight dynamics and control strategy for electric solar wind sails based on the nodal position finite element method, where the coupling effects between tether dynamics and electrical field are considered. A modified throttling control strategy is proposed to control the attitude of electric sails by modulating individual tether voltage synchronously with the spinning motion of the sails. The effects of four critical physical parameters: tether numbers, tether length, sail spin rate, and mass of remote units are investigated. The results show that the effect of the relative velocity of the solar wind has a significant effect on the spin rate of the sail in attitude maneuvering, which in turn affects the attitude dynamics and orbit motion of the sail. Numerical results show that the proposed control strategy work successfully stabilizes the spin rate of sail when the TI type sail is adopted.

Nomenclature

c_d, c_{min}, c_{max}	=	Desired, lower bound and upper bound relative ratio of spin rate.
$\boldsymbol{C}_e$	=	Damping matrix of tether
$\boldsymbol{F}_c$	=	Vectors of Coulomb force exerting on tether
$\boldsymbol{F}_k$	=	Vectors of force term due to the elasticity of tether
$\boldsymbol{F}_g$	=	Vectors of gravitational force exerting on tether
$\boldsymbol{K}_e$	=	Stiffness matrix of tether

* Postdoctoral Fellow. Department of Mechanical Engineering, York University. lgq1984@yorku.ca

† Professor, Department of Mechanical Engineering, York University. gzhu@yorku.ca. AIAA Associate Fellow and lifetime member (Corresponding Author).

‡ Doctoral candidate. Department of Earth and Space Science and Engineering, York University.

$L_{e,k}$ = Instantaneous length of k-th element, m

m_l = The number of main/auxiliary tethers of E-sail.

m_p = Mass of proton, 1.67262×10^{-27}, kg

$\boldsymbol{M}_e$ = Mass matrix of tether

n_e = Electron density in solar wind, m^{-3}

$\boldsymbol{n}_s$ = Unit vector normal to the spin plane

$\boldsymbol{n}_z^b$ = Unit vector spin axis in the body fixed frame

q_e = Charge of electron, 1.60218×10^{-19}, C

R = Distance from center of mass of E-sail to the center of Sun, m

T_e = Temperature of electron in solar wind, eV

V_{sw} = Solar wind velocity, m/s

X, Y, Z = Position coordinates, m

ε_0 = Permittivity of vacuum, 8.84542×10^{-12}, F/m

λ_e = Two times of Debye length $2\sqrt{\varepsilon_0 T_e / n_e q_e^2}$, m

Φ_b = Base voltage of main tether, V

Φ_p = Voltage of p-th main tether, V

$\Phi_{p,min}$, $\Phi_{p,max}$ = Minimum and maximum voltage of p-th main tether, V

I. Introduction

LECTRIC solar wind sail (E-sail) is an innovative propulsion technology that generates thrust by deflecting solar wind protons [1-3]. It has been proposed for various interplanetary explorations for asteroids, cometary, terrestrial planets [4], non-Keplerian orbits [5], and out-solar systems [6]. A typical E-sail consists of a main spacecraft hub connected with multiple long and thin conductive tethers (referred to as 'main tethers' in the rest of this paper) in a hub-spoke like configuration. The geometrical configuration is maintained by centrifugal forces in the main tethers resulting from spinning the E-sail around the main spacecraft hub. These spinning main tethers are positively charged by a solar-powered electron gun at the main spacecraft hub to form an electrostatic field over a large circular area – the spin plane [3], which deflects the trajectory of incident protons in the solar wind and generates thrust

acting on the E-sail through momentum exchange between deflected proton and the E-sail [3, 7-9]. This thrust, as shown in Fig. 1, is proportional to the distance R from the center of Sun by $1/R^{7/6}$ [2, 3]. Comparably, the thrust provided the protons in a solar sail decays by $1/R^2$ [10]. Thus, the E-sail takes advantage of solar sails [11] and solar wind magnetic sails [12] while avoiding their disadvantages - faster decade rates. This makes the E-sail a competitive alternative to the solar and magnetic sails in terms of lightweight [13], propellantless [1], longer operational life [3], and superior maneuverability [14]. The current work focuses on the attitude dynamics and control of E-sail.

The attitude of a spinning E-sail can be maneuvered by tilting the sail angle similar to the solar photon sail [15, 16]. The past ten years have witnessed many control methodologies in the literature for maneuvering the attitude of solar photon sail based on the idea of keeping an offset between the center of mass (CM) and the center of solar radiation pressure (CP). These methods can be categorized in terms of the structural rigidity of solar photon sail, namely, rigid or non-rigid solar photon sails. For the rigid solar photon sail, many attitude control methods have been proposed by moving the positions of CM and CP, for instance, control vane method [17], gimbaled mass method [18], sliding mass method, and shifted/tilted wings [19]. For the non-rigid solar photon sail, attitude control methods based on the shift of CP have been proposed, such as the reflectivity control device (RCD) method [20] and the blade device method [21]. Considering the fact that the diameter of each main tether is at the micrometer level and the spin plane of E-sail is held only by the centrifugal force in tethers and tip masses, the flexibility of tether can play a significant role in the dynamics of E-sail [13]. Therefore, as shown in Fig. 1, the attitude control methods for the non-rigid spinning solar photon sail could be potentially applied in the attitude control of E-sails. As pointed out in Refs.[2, 3, 22], the Coulomb force exerting on the main tethers depends on temperature and density of electron, solar wind speed, and biased voltage of main tethers. Among them, the temperature and density of electron and solar wind speed are the environmental parameters and are not controllable. Thus, the torque for attitude

maneuvering of the E-sail can only be generated by modulating the biased voltage of each main tether individually [23-26]. This approach was first investigated by a scale-factor method where main tethers were simplified as spherical pendulums. However, it is found that the voltage modulation generated a net deceleration or acceleration of spin rate for inward or outward spiraling orbits, respectively [24, 26, 27]. To understand the dynamics behind the variation of the spin rate due to voltage modulation, a throttling factor method was proposed where main tethers were represented more accurately by discretized elastic wires [25, 26]. It was found that a thrust component in the spin plane was generated by the voltage modulation [23, 28, 29], resulting in an increase of spin rate up to 25% from its initial value if the E-sail is inclined 45 degrees with respect to the solar wind [25]. To reduce the variation of spin rate in the thrust vectoring, three design improvements were proposed. The first design consists of applying a counter-thrust with the remote units to balance the torque resulting from the thrust component in the spin plane [3, 26]. To avoid collision between main tethers in this process, remote units are connected by non-conductive and equal-length auxiliary tethers. The second is to assemble photonic blades between main tethers and remote units [27, 30]. The remote units are either connected with non-conductive auxiliary tethers or not. In the third (called TI type), all main tethers are connected with charged auxiliary tethers at the remote units where main tethers are electrically connected to auxiliary tethers at every two main tethers [25, 26]. Among these three design improvements, the TI type is the most promising due to its simple design and high technology readiness level [25]. Recently, a control strategy of a rotating barbell E-sail has been studied, where the tether is discretized into a series of lumped mass-spring-damper model. The voltage modulation of each tether is used to maneuver. No attitude dynamics were considered. However, the barbell E-sail is very simple, and it had a few tethers, no auxiliary tethers, and the interaction between the main tethers was not considered [31]. The attitude dynamics of E-sail is studied by modeling main tethers with a dumbbell model, where the spin rate is assumed sufficient to keep the main tethers taut [32]. However, the model cannot describe tether tension variation due to spin rate change in the attitude-maneuver phase [24, 25]. To

overcome the limitation, the catenary theory is used to study the effect of tether deflection on the attitude dynamics of E-sail [29, 33]. However, the remote units are not included in the study and the approach is only suitable for small in-plane angles. To the best knowledge of authors, the dynamics of E-sail in the attitude maneuver by thrust vectoring has not been investigated by considering the full tether dynamics.

In this paper, the dynamics and control of thrust vectoring for E-sail in the attitude maneuver are thoroughly investigated by considering the elastic and transverse oscillation of all tethers. Based on the finding of full dynamic responses, a new control strategy for thrust vectoring is proposed with four critical physical parameters: the number, length, and spin rate of main tethers and the mass of remote units. The results show that a high-fidelity tether model is required to accurately represent the dynamics of E-sail and the proposed control strategy is effective in controlling the attitude of the E-sail by thrust vectoring.

II. Dynamics of Electric Solar Wind Sail

A. High-Fidelity Model of the E-sail

Consider a spinning E-sail as shown in Fig. 2a, where the main and auxiliary tethers are divided into multiple two-node straight finite elements and modeled by the nodal position finite element method (NPFEM) [22, 34, 35]. Each tether element is assumed as a tensile member only with zero compressive stiffness due to the incompressibility of E-sail tethers [13]. Since the length of main tethers is several orders of magnitude greater than the size of the central spacecraft hub and remote units, the central spacecraft hub and remote units are modeled as lumped masses with attitude dynamics ignored [14]. The motion of E-sail is described in four coordinate frames: the global heliocentric-ecliptic inertial frame ($O_g X_g Y_g Z_g$), the orbital frame ($O_o X_o Y_o Z_o$), the local frame of the tether element ($otnb$), and the frame fixed to E-sail describing the spin plane ($O_o X_b Y_b Z_b$), see Fig. 2a. The definition of first three coordinate systems has been given in our previous work [22]. In the current paper, the body-fixed

frame ($O_oX_bY_bZ_b$) is coincided with the orbital frame initially. As shown in Fig. 2a, two angles are defined to describe the motion of the spin plane of E-sail, namely the in-plane angle α (rotating around the Y_o axis), and the out-of-plane angle β (rotating around the X_o' axis that is the X_o axis after the first rotation). In the current paper, it is assumed that the out-of-plane angle of E-sail is zero degree for simplicity, and the E-sail is rotating about the positive Z_o axis.

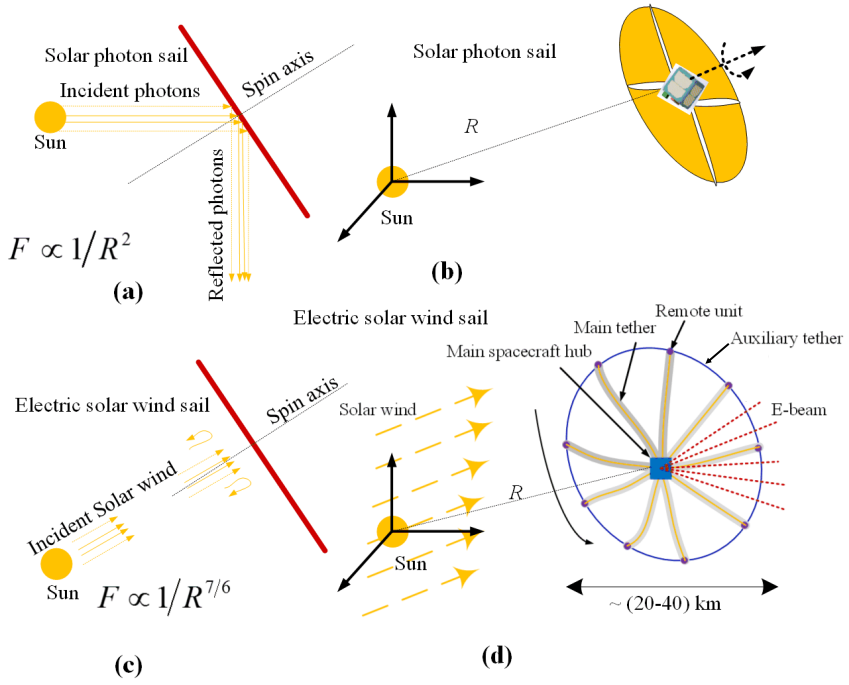

Fig. 1 Schematics of solar photon sail and E-sail.

Assuming the tether of E-sail is divided into *n* tensile elements, and the equation of motion of one element can be derived by the principle of virtual work [22, 35]. Taking the *k-th* element as an example,

$$\boldsymbol{M}_{e,k}\ddot{\boldsymbol{X}}_{e,k}+\boldsymbol{C}_{e,k}\dot{\boldsymbol{X}}_{e,k}+\boldsymbol{K}_{e,k}\boldsymbol{X}_{e,k}=\boldsymbol{F}_{c,k}+\boldsymbol{F}_{g,k}+\boldsymbol{F}_{k,k} \tag{1}$$

where $\boldsymbol{X}_{e,k}=\left(X_k,Y_k,Z_k,X_{k+1},Y_{k+1},Z_{k+1}\right)^T$ is the vector of position coordinates of element nodes with subscripts *k* and *k*+1 denoting the nodes of the *k-th* element. The overdot denotes the derivative with respect to time. The detailed expression of mass and stiffness matrices can be found in Ref. [34]. The Rayleigh damping model is used to calculate the damping matrix $\boldsymbol{C}_{e,k}$ [36], and the coefficients

relate to this model will be given in the simulation section. Note that the term $\boldsymbol{F}_{k,k}$ is resulting from the stiffness matrix of the traditional finite element method when transforming the state variables from nodal displacement to nodal position [22, 34, 37]. Thus, the stiffness matrix $\boldsymbol{K}_{e,k}$ in Eq.(1) is a rank deficient matrix.

The vector of Coulomb force can be obtained by integrating along with the element,

$$\boldsymbol{F}_{c,k} = \int_0^{L_{e,k}} \boldsymbol{N}^T \boldsymbol{T}_{l2g} \boldsymbol{f}_c^l ds \tag{2}$$

where $\boldsymbol{N}$ is the linear shape function matrix with superscript *T* representing the transpose of a matrix [22], $\boldsymbol{T}_{l2g}$ is the transformation matrix from the local frame to the global frame [22] , and $\boldsymbol{f}_c^l$ is the Coulomb force per unit length expressed in the local frame as [2, 3],

$$\boldsymbol{f}_c^l = K_c m_p V_{sw}^2 \sqrt{n_e \varepsilon_0 T_e} \Big/ \left\{ q_e \sqrt{\exp\left[m_p V_{sw}^2 / \left(q_e \Phi_p \right) \ln\left(\lambda_e / r_w \right) \right] - 1} \right\} \tag{3}$$

where $K_c = 6.18$ is a constant value obtained by the numerical simulation based on the particle-in-cell method [2, 3]. The formula presented in Refs. [8, 22] is used to evaluate the values of n_e and T_e . Φ_p is the voltage of *p-th* main tether that is calculated as Eq. (9). The gaussian integration method is used to obtain the distributed Coulomb force, and five Gaussian integration points is used.

Once the equation of motion of the *k-th* element is obtained, the equations of motion for the *n* elements (whole E-sail) can be obtained by assembling Eq. (1) with the standard assembly procedure in the conventional finite element method [22, 34, 36], such as,

$$\boldsymbol{M}_e \ddot{\boldsymbol{X}}_e + \boldsymbol{C}_e \dot{\boldsymbol{X}}_e + \boldsymbol{K}_e \boldsymbol{X}_e = \boldsymbol{F}_c + \boldsymbol{F}_g + \boldsymbol{F}_k \tag{4}$$

where $\boldsymbol{M}_e$ is a hybrid mass matrix by combining the mass matrix of tether and the masses of main spacecraft hub and remote units adding as lumped masses.

The detail explanation for obtaining the initial condition of a spinning E-sail is presented in Ref. [22]. With having the initial condition, the Eq. (4) can be numerically solved by the implicit 4th order

Runge-Kutta Gaussian-Legendre scheme with a symplectic property that is suitable for long-term dynamic analysis [22, 34, 35].

B. Attitude Motion of the E-sail

The attitude of a spinning E-sail is described in the orbital coordinate system through a set of angles (α and β) of spin axis or the normal vector of spin plane as shown in Fig. 2a, such that,

$$\begin{aligned} \alpha &= ar\tan\left(\boldsymbol{n}_{s,x}^{o} / \boldsymbol{n}_{s,z}^{o}\right) \\ \beta &= ar\tan\left(\boldsymbol{n}_{s,y}^{o} \Big/ \sqrt{\left(\boldsymbol{n}_{s,x}^{o}\right)^2 + \left(\boldsymbol{n}_{s,z}^{o}\right)^2}\right) \end{aligned} \tag{5}$$

where superscripts $(\ )^{o}$ and $(\ )^{g}$ represent the term expressed in the orbital and global heliocentric-ecliptic inertial coordinate systems, respectively. $\boldsymbol{n}_s^o = \left(\boldsymbol{n}_{s,x}^{o}, \boldsymbol{n}_{s,y}^{o}, \boldsymbol{n}_{s,z}^{o}\right)^T = \boldsymbol{T}_{g2o}\boldsymbol{n}_s^g$ is the unit vector of spin axis or the unit vector normal to the spin plane of the E-sail, and $\boldsymbol{T}_{g2o} = \boldsymbol{T}_{o2g}^T$ is the transformation matrix from the global heliocentric-ecliptic inertial coordinate system to the orbital coordinate system [22].

It should be mentioned that the unit vector $\boldsymbol{n}_s^g$ or $\boldsymbol{n}_s^o$ is a variable that is usually determined by solving an differential equation about the angular momentum of E-sail as presented in Ref. [25]. To simplify the process, we propose an alternative direct approach based on the geometry aspect. Assume there exists a stable spin plane when an attitude control strategy is applied [32]. Then, the spin axis or unit vector $\boldsymbol{n}_s^g$ normal to the spin plane can be calculated,

$$\boldsymbol{n}_s^g = \left(\boldsymbol{X}_{21}^{g} \times \boldsymbol{X}_{23}^{g}\right) \Big/ \left\| \boldsymbol{X}_{21}^{g} \times \boldsymbol{X}_{23}^{g} \right\| \tag{6}$$

where $\boldsymbol{X}_{21}^{g} = \boldsymbol{X}_{2}^{g} - \boldsymbol{X}_{1}^{g}$ and $\boldsymbol{X}_{23}^{g} = \boldsymbol{X}_{2}^{g} - \boldsymbol{X}_{3}^{g}$. Here, $\boldsymbol{X}_{j}^{g}\ (j = 1, 2, 3)$ are the vectors of the position of three chosen remote units with superscript "g" denoting in the global inertial system, see Fig. 2b.

In the attitude maneuvering process, the target or desired attitude angles of E-sail (α_t and β_t) are

assumed to give. Then, the target normal vector of the spin plane in the global coordinate system can be expressed as,

$$\boldsymbol{n}_t^g = \boldsymbol{T}_{o2g}\boldsymbol{n}_t^o = \boldsymbol{T}_{o2g}\boldsymbol{T}_{b2o}\left(\alpha_t, \beta_t\right)\boldsymbol{n}_t^b \tag{7}$$

where $\boldsymbol{n}_t^b = \begin{pmatrix} 0 & 0 & 1 \end{pmatrix}^T$ is a known unit vector expressed in the body-fixed frame, $\boldsymbol{T}_{b2o}\left(\alpha_t, \beta_t\right)$ is the transformation matrix from the body-fixed coordinate system to the orbital coordinate system with the given angles (α_t and β_t),

$$\boldsymbol{T}_{o2b}\left(\alpha_t, \beta_t\right) = \begin{bmatrix} \cos\alpha_t & 0 & -\sin\alpha_t \\ \sin\alpha_t \sin\beta_t & \cos\beta_t & \cos\alpha_t \sin\beta_t \\ \sin\alpha_t \cos\beta_t & -\sin\beta_t & \cos\alpha_t \cos\beta_t \end{bmatrix} \tag{8}$$

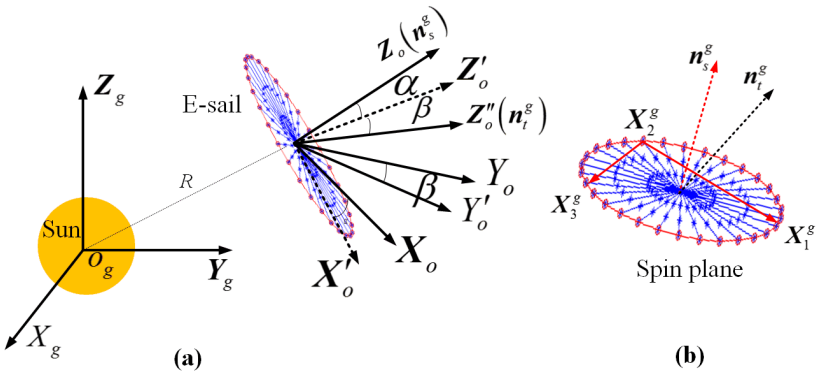

Fig. 2 Schematic diagram of E-sail and tefinition of unit normal vector of spin plane.

C. Attitude Control Strategy

As mentioned in Refs. [23-25], a simple and intuitive attitude control strategy for E-sails can be achieved by modulating the voltages of each charged tether individually because the thrust is directly proportional to the applied voltage as presented in Section A. Taking the *p-th* ($p = 1, \ldots, m_l$) main tether as an example, the voltage $\Phi_p\left(p = 1, \ldots, m_l\right)$ can be expressed as [25],

$$\Phi_p = \left(f_{1,p} f_{2,p} f_{3,p} f_{4,p}\right)\Phi_b \tag{9}$$

where, and ($f_{1,p}$, $f_{2,p}$, $f_{3,p}$, $f_{4,p}$) are the control factors related to the unit normal vector of spin

plane or attitude of E-sail, change of relative ratio of spin rate ($\left|\boldsymbol{n}_s^g\right| / \left|\boldsymbol{n}_{s,or}^g\right|$), spin plane holding, and artificial damping for the oscillation of tethers. They are defined as follows,

$$f_{1,p} = \max\left[0,\ \left(1 - u_1 \boldsymbol{e}_{r,p}^g \cdot \left(\boldsymbol{n}_t^g \times \boldsymbol{n}_s^g\right) / \left\|\boldsymbol{n}_t^g \times \boldsymbol{n}_s^g\right\|\right)\right] \tag{10}$$

$$f_{2,p} = \max\left\{c_{\min},\ \min\left[\pm u_2 \left(c_d - \left\|\boldsymbol{n}_s^g\right\| / \left\|\boldsymbol{n}_{s,or}^g\right\|\right) \boldsymbol{v}_p^g \cdot \boldsymbol{n}_{sw}^g,\ c_{\max}\right]\right\} \tag{11}$$

$$f_{3,p} = 1 \Big/ \left\|\left(\boldsymbol{n}_z^b - u_3 \boldsymbol{e}_{r,p}^b\right) / \left\|\boldsymbol{n}_z^b - u_3 \boldsymbol{e}_{r,p}^b\right\|\right\| \tag{12}$$

$$f_{4,p} = 1 + \min\left(0,\ u_4 \sum_{p=1}^{m_l} \boldsymbol{v}_{p,z}^b \Big/ \sum_{p=1}^{m_l} \left\|\boldsymbol{v}_p^b\right\|\right) \tag{13}$$

where u_i $(i = 1,2,3,4)$ are the control gains, and the control gains should be tuned based on the trail and error for the detailed physical parameters of E-sail. ($\boldsymbol{e}_{r,p}^g$, $\boldsymbol{e}_{r,p}^b$) and ($\boldsymbol{v}_p^g$, $\boldsymbol{v}_p^b$) are the unit vectors of position and velocity of *p-th* remote unit relative to the main spacecraft hub (1st node) in the global and body-fixed frames, $\boldsymbol{n}_s^g$ and $\boldsymbol{n}_{s,or}^g$ are the instant and initial normal vectors of spin plane, respectively. $\boldsymbol{n}_{sw}^g = \boldsymbol{T}_{o2g} \boldsymbol{n}_{sw}^o$ with $\boldsymbol{n}_{sw}^o$ being the unit vector of the solar wind direction in the orbital plane frame, the minus/plus signs are switch for even/odd-numbered main tethers respectively.

The factor f_1 is active for turning the spin plane when the vectors $\boldsymbol{n}_t^g$ and $\boldsymbol{n}_s^g$ don't coincide with each other $\boldsymbol{n}_t^g \neq \boldsymbol{n}_s^g$. The phase difference of each main tether is described by the angle between the unit vector $\boldsymbol{e}_{r,p}^g$ and the unit vector $\left(\boldsymbol{n}_t^g \times \boldsymbol{n}_s^g\right) / \left\|\boldsymbol{n}_t^g \times \boldsymbol{n}_s^g\right\|$. For the factor f_2, the instantaneous spin rate relative to the desired value is index by $c_d - \left\|\boldsymbol{n}_s^g\right\| / \left\|\boldsymbol{n}_{s,or}^g\right\|$, and the plus and minus signs are assigned for the T-tethers and I-tethers, respectively. For the factor f_3, the deviation of each tether away from the spin plane is described by the difference between the spin axis aligned vector $\boldsymbol{n}_z^b$ and the unit vector $\boldsymbol{e}_{r,p}^b$ of remote units relative to the main spacecraft hub. For the damping related factor f_4, we measure

the spin aligned speed $\boldsymbol{v}_{p,z}^{b}$ of the remote units relative to the main spacecraft hub, and they are averaged over all the remote units. Furthermore, the measurement of the velocity of the remote units are calculated by the finite difference method based on the angular position of remote units.

Based on the principle for saving the onboard computing power of main spacecraft hub, the update interval time is 2 s for the control factors f_1 and f_2, 30 s for the control factor f_3, and 1500 s for the control factor f_4. Besides, the voltage of a charged tether should be subject to upper and lower bounds due to the limited capability of the power supply system of E-sail,

$$\Phi_{p,\min} \le \Phi_p \le \Phi_{p,\max} \tag{14}$$

III. Simulation Results and Discussion

The parameters of the employed implicit solver, the maximum iteration number and the tolerance of residual error of iteration, are set 100 and 10^{-10}, respectively. The physical parameters of a typical E-sail are listed in Table 1 [13] and the parameters of proposed control law are shown in Table 2. The gain of the proposed controller is given based on the trial and error for the physical parameters given in Table 1. In the current paper, the main and auxiliary tethers are modeled with four and one tether elements respectively, after the trade-off analysis between accuracy and computational cost. The time step-size is 0.01s and the simulation time duration is 691,200 s (8 days). The solar wind is assumed propagating radially from the Sun at 400 km/s [22]. The effect of the velocity of the solar wind with respect to tether is not considered temporally except it is specifically pointed out.

Here, the structural damping of the tether is not considered due to the lack of experimental data in the space environment, and it can be done by setting the coefficients in the Rayleigh damping model to zero [36]. Nonetheless, the damping effect stabilizes the numerical solution of E-sail dynamics. Thus, the neglect of damping will not affect the validation of the current analysis.

Table 1 Physical properties of E-sail.

Parameters	Values
Mass of main satellite (*kg*)	200

Number of main tethers (auxiliary tethers)	18 (18)
Base voltage of charged tether (kV)	20
Minimum/Maximum voltage of charged tether (kV)	0/40
Length of main tether (km)	10
Material type of main tether (auxiliary tether)	Aluminum (Kapton)
Material density of main tether (kg/m^3)	2700
Material density of auxiliary tether ($kg/m3$)	1420
Elastic modulus of main tether (GPa)	100
Elastic modulus of the auxiliary tether (GPa)	2.5
Diameter of main tether (m)	7.38×10^{-5}
Mass of remote unit (kg)	1.5
Width of auxiliary tether (m)	0.03
Thickness of auxiliary tether (μm)	12.7
Initial orbital radius of E-sail (AU)	1.0
Initial spin rate of E-sail (deg/s)	0.24

Table 2 Parameters of proposed control law.

Parameters	Values
Gain of spin plane attitude u_1	35.0
Gain of spin rate change u_2	100.0
Gain of attitude keeping u_3	1.0
Gain of tether oscillation damping u_4	3.0
Target in-plane angle (deg)	20.0
Target out-of-plane angle (deg)	0.0
Desired relative ratio of spin rate r_g	1.0
Lower bound of relative ratio of spin rate c_{min}	-0.5
Upper bound of relative ratio of spin rate c_{max}	0.5

Table 3 Simulation cases in parametric study.

Name	Number of main tethers	Length of main tether (km)	Spin rate (rad/s)	Mass of remote unit (kg)
Case A	6	10	0.24	1.5
Case B	12	10	0.24	1.5
Case C	18	10	0.24	1.5
Case D	18	15	0.24	1.5
Case E	18	20	0.24	1.5
Case F	18	10	0.12	1.5
Case G	18	10	0.18	1.5
Case H	18	10	0.30	1.5
Case I	18	10	0.24	0.5
Case J	18	10	0.24	3.0

A. Validation of Proposed Evaluation Method for Orientation of Spin Axis

In this section, the approximation method (called the proposed method) to evaluate the normal vector of the spin plane based on the geometrical aspect of E-sail is verified. Four numerical simulations are carried out for an E-sail with 18 main tethers in two scenarios, one is the in-plane attitude motion, and the other one is three-dimensional attitude motion including both the in-plane and out-of-plane motions. As shown in Fig. 3, six candidates of triangles formed by remote units are selected to calculate the normal vector of the spin plane. The control gains of proposed control law are listed in Table 2, except for the control gain u_2 that controls the spin rate variation. Here u_2 is set zero to observe the natural variation of spin rate in the attitude maneuver process. For the first scenario, the target in-plane, and out-of-plane angles (α_t and β_t) are set as 20 and 0 degrees, respectively. For the second scenario, the α_t and β_t are set as 15 and 5 degrees, respectively.

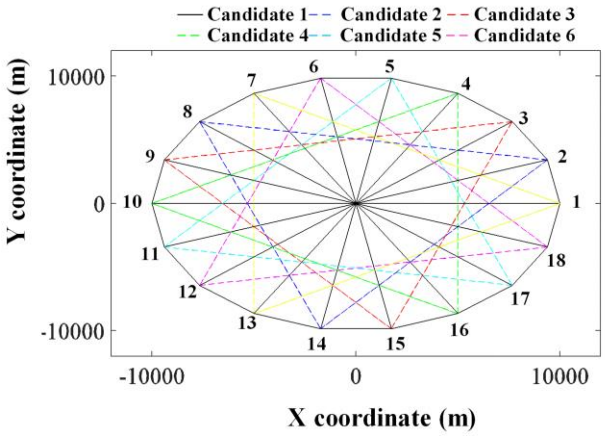

Fig. 3 Triangle candidates represent spin plane of a typical E-sail.

The results are compared with the reference method in Ref. [25], in which the spin axis of normal vector of the spin plane is obtained by solving a differential equation of angular momentum of E-sail. Here, the vector representing the spin axis is determined through simple algebraic manipulation of these six candidate triangles based on Eq. (5). Figure 4 shows the comparison of the in-plane and out-of-plane angles at these two scenarios. It shows the results of the proposed method agree very well with the result from the reference method with negligible differences. The results of both methods agree with each other. It can be concluded that the attitude of E-sail can be evaluated with enough

accuracy by the proposed method without solving the differential equation of the angular momentum of E-sail. For the sake of simplicity, the triangle formed by 1st, 7th, and 14th remote units is chosen to calculate the normal vector of the spin plane in the following simulation cases.

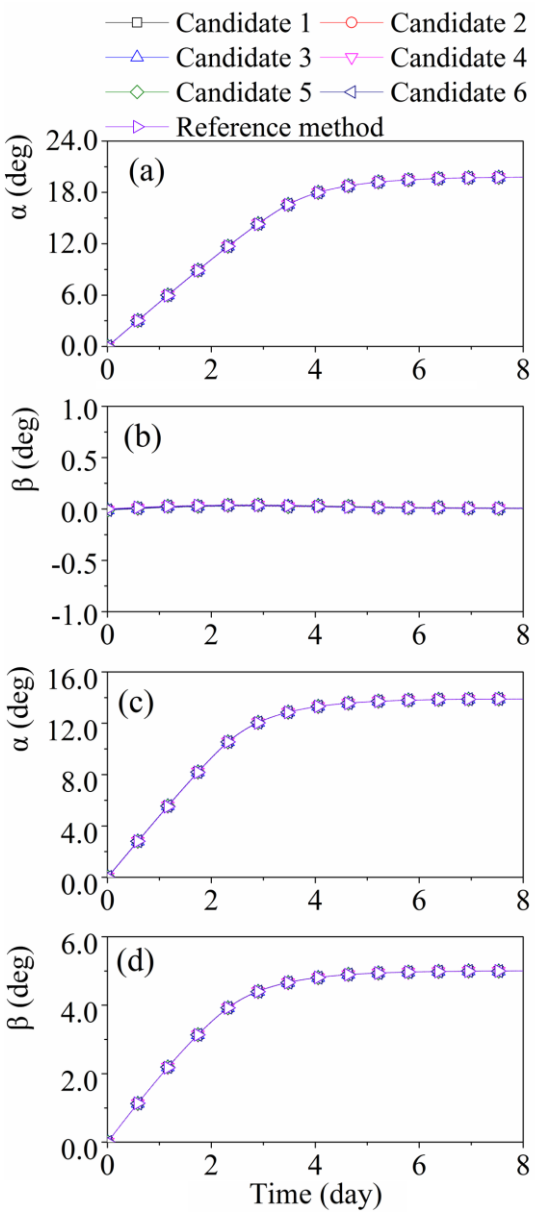

Fig. 4 Variation of attitude angle between the proposed and reference methods. (a), (b): (α_t = 20 deg, β_t = 0 deg). (c) (d): (α_t = 15 deg, β_t = 5 deg).

Table 4 Results in terms of T_{at} and S_{at} in parametric study.

Name	Case A	Case B	Case C
T_{at} (*day*)	11.6	8.4	6.5

D_{at} (AU)	2.28×10^{-5}	4.44×10^{-5}	6.49×10^{-5}	
Name	**Case C**	**Case D**	**Case E**	
T_t (day)	6.5	8.2	9.6	
D_{at} (AU)	6.49×10^{-5}	8.95×10^{-5}	11.10×10^{-5}	
Name	**Case F**	**Case G**	**Case C**	**Case H**
T_t (day)	3.8	5.8	6.5	9.0
D_{at} (AU)	6.77×10^{-5}	6.62×10^{-5}	6.49×10^{-5}	6.38×10^{-5}
Name	**Case I**	**Case C**	**Case J**	
T_t (day)	5.4	6.5	11.2	
D_{at} (AU)	7.14×10^{-5}	6.49×10^{-5}	5.74×10^{-5}	

B. Parametric Study of Maneuverability of E-sail

To investigate the influence of physical parameters of E-sail on the orbital and attitude dynamics, as listed in Table. 3, a series of numerical simulations are conducted. The parameters considered in this work include the number of main tethers, the length of each main tether, the initial spin rate, and the mass of remote units. However, the proposed spin rate controller is not considered by setting the gain u_2 to zero to allow the spin-rate to vary naturally in E-sail attitude maneuvering. In this section, only the in-plane attitude motion of E-sail is considered, and the α_t and β_t are set as 20 and 0 degrees, respectively if not be specified. As shown in Fig. 4(b) previously, the out-of-plane angle β is close to zero and it can be ignored and will be not plotted in the rest of this paper. The influence of system parameters is examined by the two new defined criteria: (i) attitude maneuver time T_{at}: the time for the attitude of E-sail from the initial state to the target state, and (ii) orbital travel distance D_{at}: the travel distance of CM of E-sail in the period of attitude maneuver.

1. Effect of Main Tether Number

A typical E-sail system may have as many main tethers as up to 100 [13, 24]. Here, the influence of the number of main tethers is investigated in three cases, where the numbers of main tether change from 6 to 18 with an increment of 6. The results are shown in Figs. 5-7 and Table 4. Intuitively, the more the main tethers of an E-sail, the high the thrust it generates. This is because the thrust is proportional to the number of main tethers. This is shown clearly in Fig. 5(d) in terms of thrust (Z_o

component of thrust). Therefore, the E-sail travels more distance at a given time, as listed in Table 4. For the attitude motion of E-sail, Figs. 5(a) and 6 show the variation of in-plane angle α and geometrical configuration of E-sail expressed in the orbital frame, respectively. A distinct difference is easily found. It reveals that the more the number of main tethers, the higher the attitude maneuverability. For instance, as listed in Table 4, the attitude maneuver time D_t reduces from 10.6 days to 6.5 days when the number of main tethers increases from 6 to 18. Figure 5(b) shows the spin rate ratio (instance/initial value) of E-sail, where the value of the spin rate is obtained by averaging angular velocities of remote units. It shows the spin rate ratio increases when the in-plane angle α reaches the target angle α_t [24, 25]. This is because a torque along the spin axis is generated when the voltage modulation of the main tethers is used. Also, the more the number of main tethers, the less the oscillation of tether in the out-of-spin plane direction. This result can be obtained by observing the oscillation of tension around the mean value, seen in Fig. 5(c). Furthermore, the same phenomenon can be observed from the geometric configuration of E-sail expressing in the body-fixed coordinate system, see in Fig. 7. Finally, it can be concluded that a large number of main tethers are preferred in terms of travel distance and attitude maneuver time.

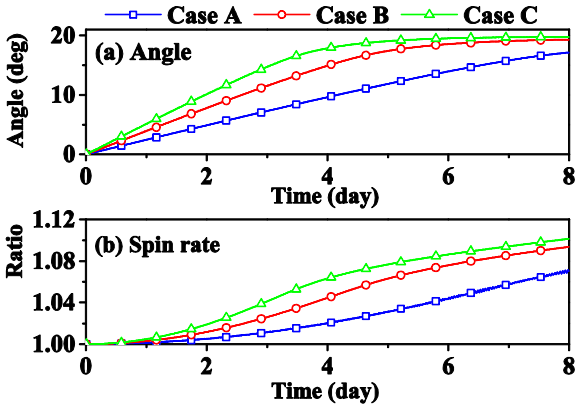

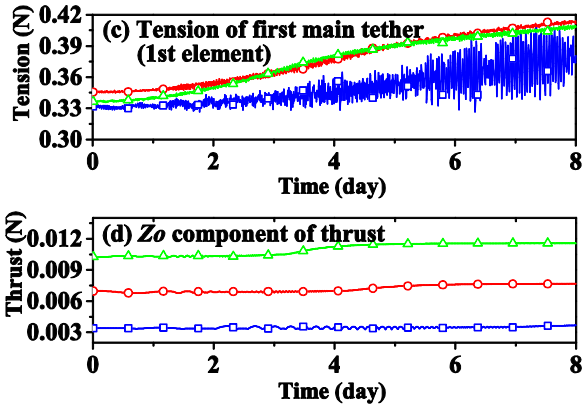

Fig. 5 Influence of main tether number on travel distance, thrust, and dynamic response of E-sail.

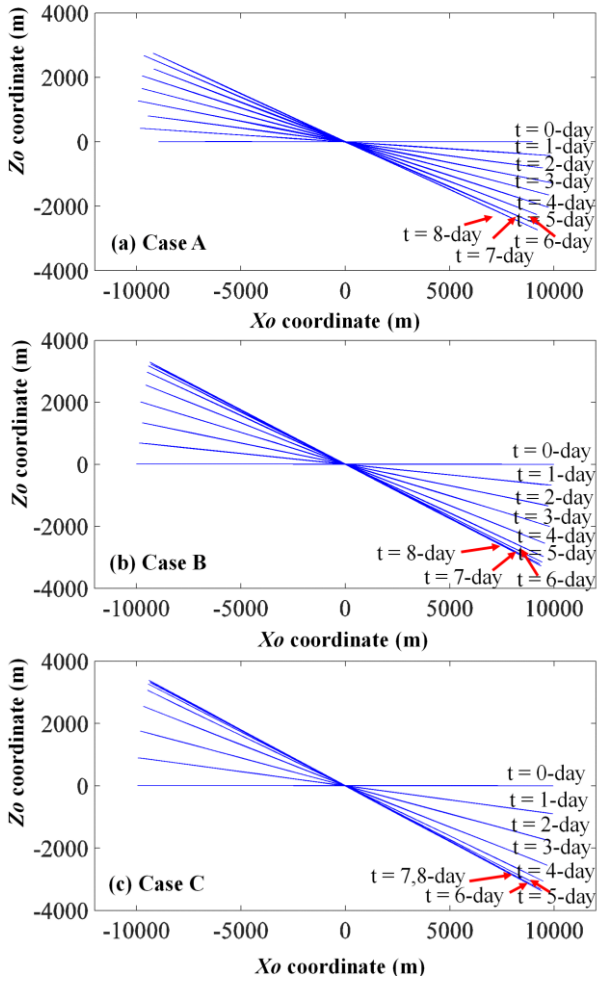

Fig. 6 Influence of main tether number on attitude of E-sail.

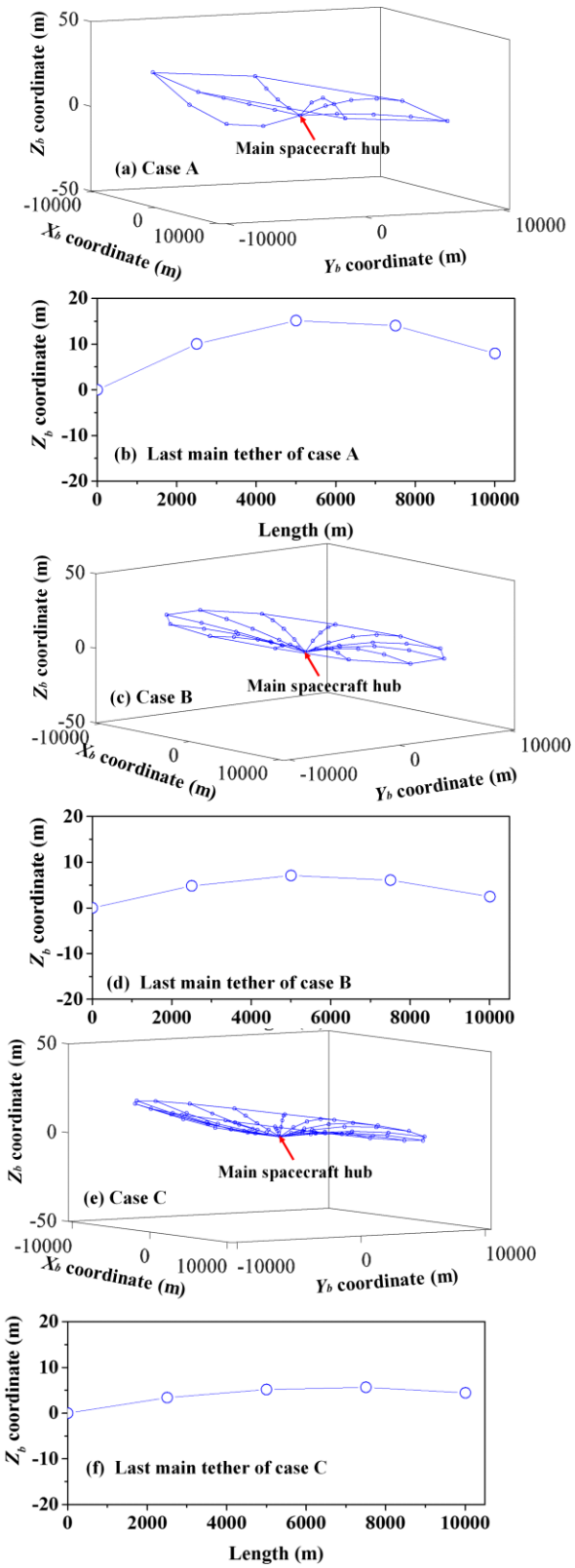

Fig. 7 Influence of main tether number on geometrical configuration of E-sail in body fixed coordinate system (4-day). (a), (c), (e): 3D view. (b), (d), (f): deflection of main tether.

2. Effect of Main Tether Length

Let the length of the main tether vary from 10 km to 20 km with an increment of 5 km [13, 25]. The results are shown in Figs. 8-10 and Table 4. As listed in Table 4, it can be easily found that the longer the main tether is, the more distance it travels. This is because the thrust is proportional to the length of the main tether, see Fig. 8(d). For the attitude motion of E-sail, as shown in Figs. 8(a) and 9, the attitude maneuver time T_{at} increases as the length of the main tethers increases. For example, T_{at} increases from 5.6 days to 9.6 days when the length of the main tethers increases from 10 km to 20 km. There are two reasons to which this phenomenon can be attributed: (i) the inertia of E-sail increases with longer tethers, and (ii) the generated thrust is controlled by tether voltage, which is bounded due to limited power source of the main spacecraft. Thus, the capability of attitude maneuver is reduced for longer main tethers when the applied voltage is bounded. Besides, as shown in Fig. 8(c), the longer is the main tether, the higher is the tether tension. As a result, the transverse oscillation of the tether is still at the same level due to the tension stiffening effect even when the length of main tether is double, see in Fig. 10. The same phenomenon of spin rate ratio (instance/initial value) can be observed in the attitude maneuver process, see Fig. 8(b). Therefore, longer main tethers are preferred for higher thrust, while shorter main tethers are preferred for attitude maneuver.

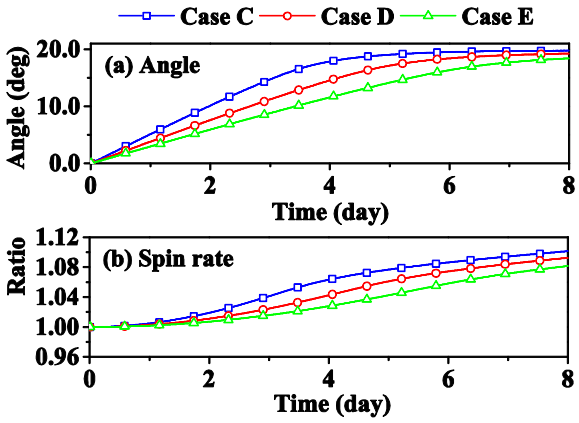

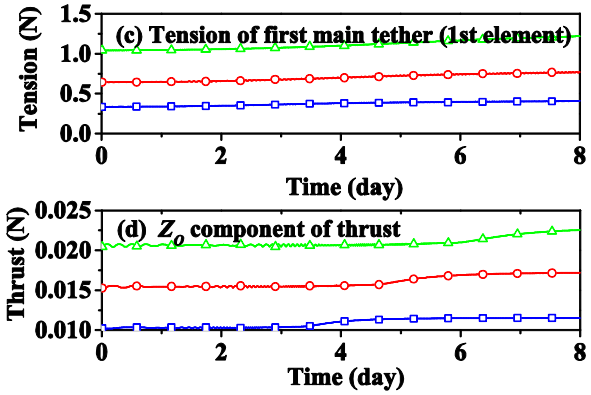

Fig. 8 Influence of length of main tether on travel distance, thrust, and dynamic response.

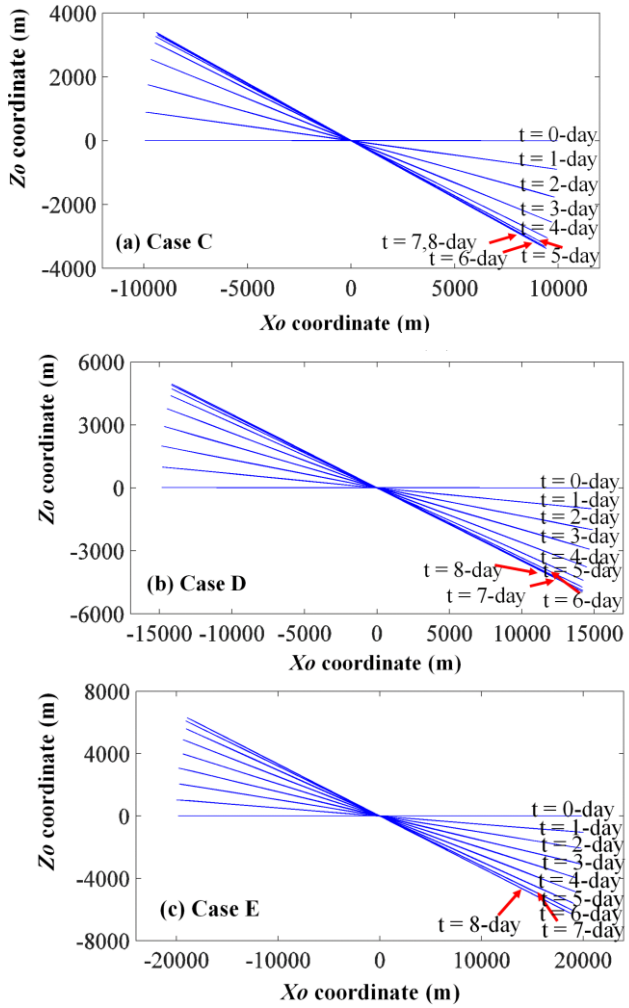

Fig. 9 Influence of length of main tether on attitude motion of E-sail.

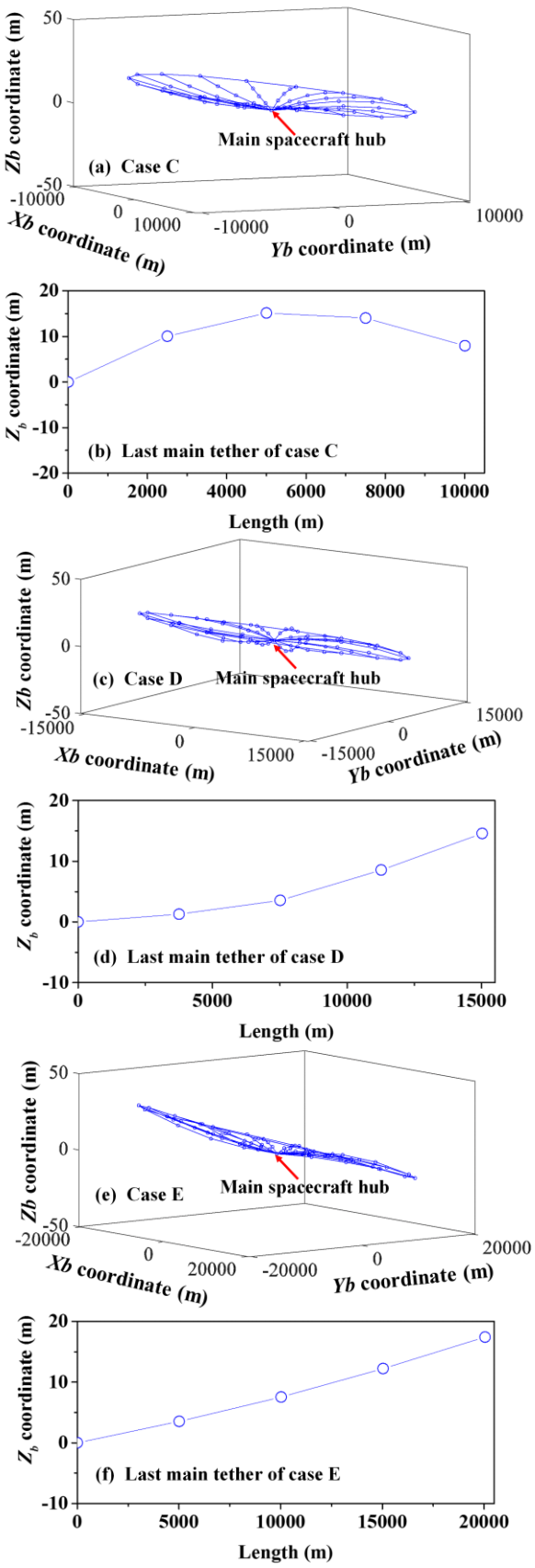
Zb coordinate (m)
50
0
-50
Main spacecraft hub
(a) Case C
-10000
0
10000
Xb coordinate (m)
-10000
0
10000
Yb coordinate (m)
Z_b coordinate (m)
20
10
0
-10
-20
(b) Last main tether of case C
0
2000
4000
6000
8000
10000
Length (m)
Zb coordinate (m)
50
0
-50
(c) Case D
Main spacecraft hub
-15000
0
15000
Xb coordinate (m)
-15000
0
15000
Yb coordinate (m)
Z_b coordinate (m)
20
10
0
-10
(d) Last main tether of case D
0
5000
10000
15000
Length (m)
Zb coordinate (m)
50
0
-50
(e) Case E
Main spacecraft hub
-20000
0
20000
Xb coordinate (m)
-20000
0
20000
Yb coordinate (m)
Z_b coordinate (m)
20
10
0
-10
(f) Last main tether of case E
0
5000
10000
15000
20000
Length (m)

Fig. 10 Influence of length of main tether on geometrical configuration of E-sail in body fixed coordinate system (4-day). (a), (c), (e): 3D view. (b), (d), (f): deflection of main tether.

3. Effect of Spin Rate

In order to avoid the tethers broken by centrifugal force, the spin rate of the E-sail system must be carefully designed not to exceed certain limit [28]. As listed in Table 3, four numerical cases are conducted to investigate the influence of the initial spin rate on its dynamics. From Table 4 and Fig.11(d), it is found that the spin rate has trivial impact on the orbital travel distance because the thrusts in four cases are at a similar level for given initial spin rates. However, the initial spin rate has a significant impact on the attitude maneuverability, see in Fig. 11(a) and Fig. 12. It reveals that the higher is the spin rate, the less is the attitude maneuverability. For example, as listed in Table 4, the attitude maneuver time D_t of case H is 2.4 times longer than the results of case F. There are two reasons to which this phenomenon can be attributed: (i) the momentum of E-sail increases as the spin rate increases, and (ii) the available thrust is bounded if the voltage on the main tether is limited by pre-defined bounds. Also, as shown in Fig. 13, it can be found that a high spin rate is beneficial for suppressing the out-of-plane transverse oscillation of tether. For example, the bending profile of the main tether decreases as the spin rate increases due to the stiffening effect by higher tether tension. Therefore, a suitable medium spin rate is preferred.

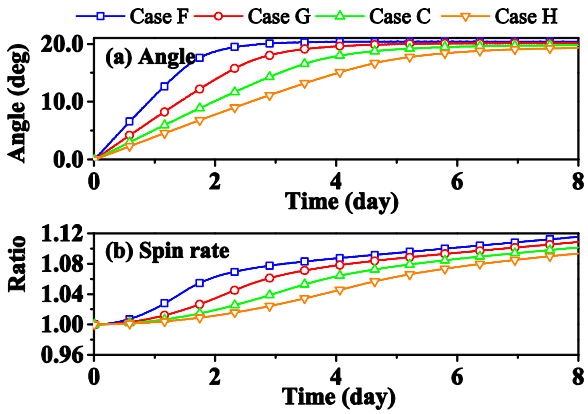

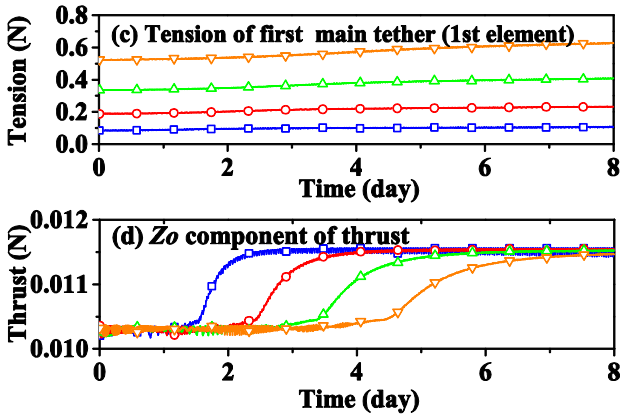

Fig. 11 Influence of initial spin rate on travel distance, thrust, and dynamic response.

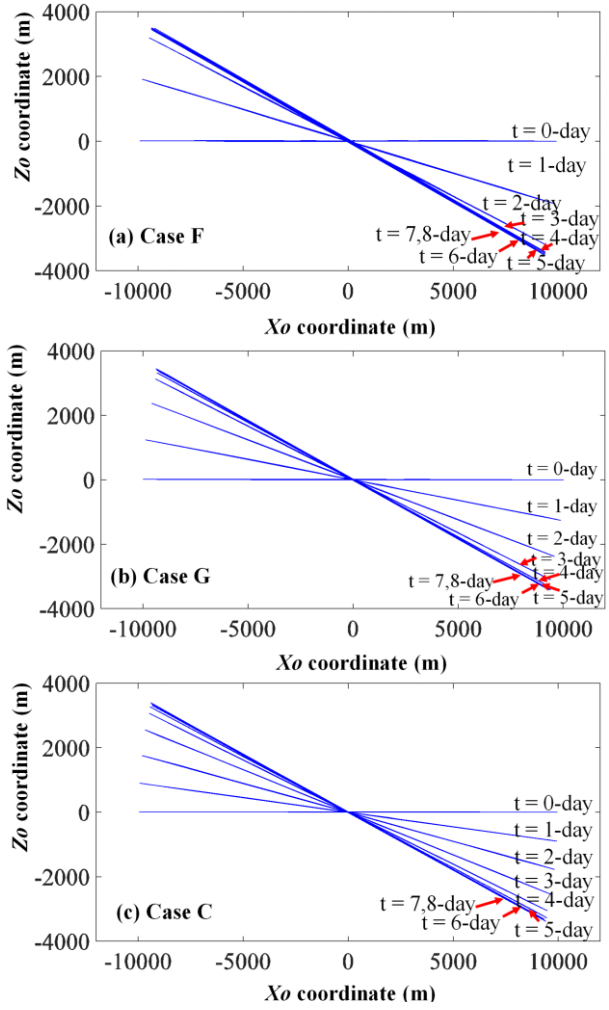

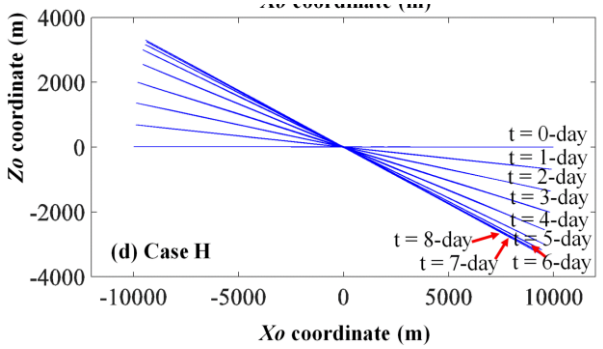

Fig. 12 Influence of spin rate on attitude motion of E-sail.

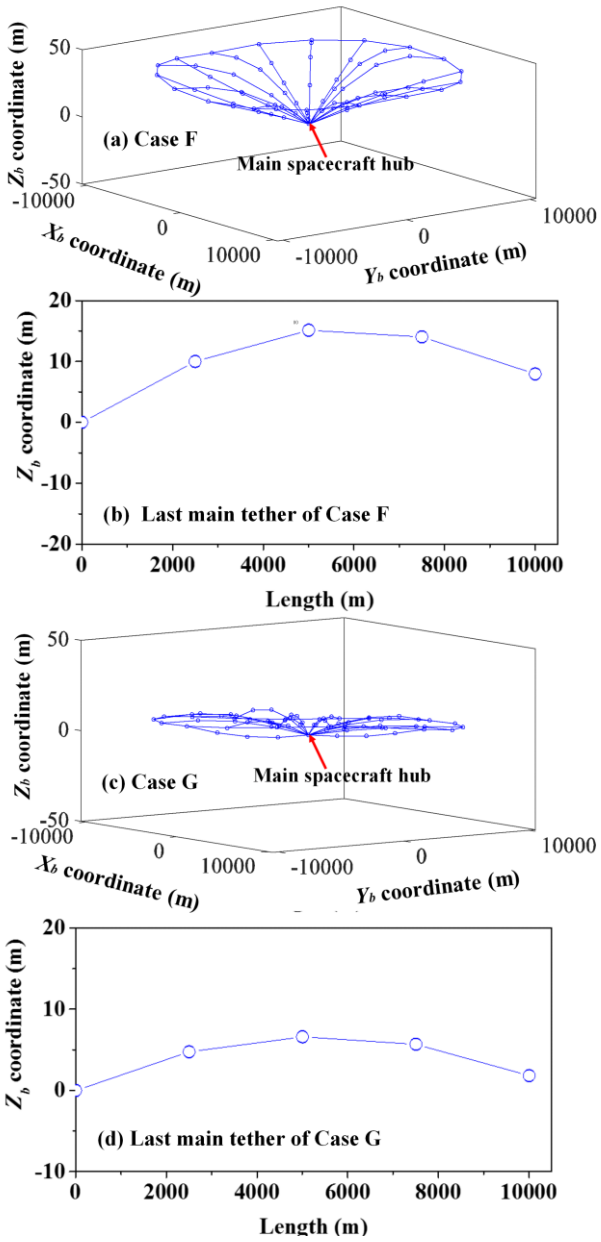

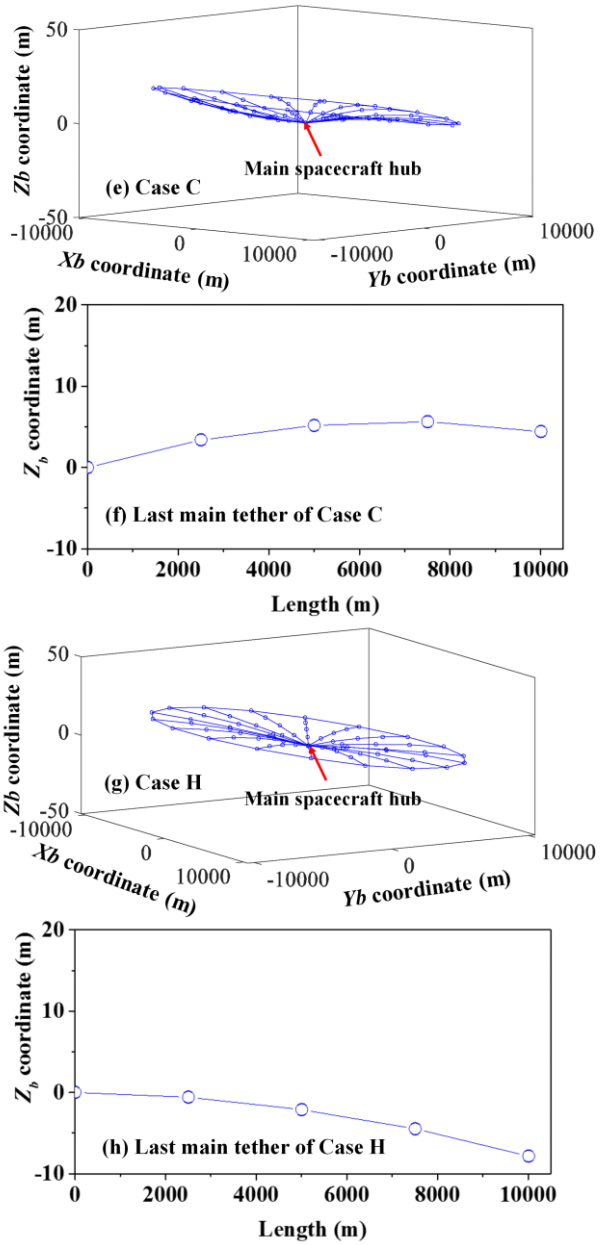

Fig. 13 Influence of spin rate on geometrical configuration of E-sail in body fixed frame (4-day). (a), (c), (e), (g): 3D view. (b), (d), (f), (h): deflection of main tether.

4. Effect of Remote Unit Mass

The remote unit is the host platform for reels for tether deployment and low thrusters for spin rate control [13]. As listed in Table 3, three numerical cases are conducted to investigate the mass of remote unit influence on the dynamics of E-sail. From Table 4, it can be found that there is a slight difference in the orbital travel distance. This is caused by the difference in the total mass of E-sail while the thrusts

are at the same level, see Fig. 14(d). However, as shown in Fig. 14(a) and Fig. 15, it shows that the lighter the mass of remote unit E-sail, the higher the attitude maneuverability. For example, as listed in Table. 4, the attitude maneuver time T_{at} of the case *J* is 2.1 times longer than the result of case *I*. The reasons are two folds: (i) the inertia of E-sail increases with heavier remote units, and (ii) the available thrust is bounded due to the upper and lower bounds applied on tether voltage. Besides, as shown in Fig. 14(c), the tension increases with the mass of remote units, which stiffens the tether and is beneficial for suppressing the out-of-spin plane oscillation of tether during the E-sail attitude maneuver phase. For example, Fig. 16 shows the Z_b coordinate of E-sail decreases as the mass of the remote unit increases. It reveals heavier remote units are helpful for keeping the spin plane.

Finally, three conclusions are obtained from this parametric study. First, the attitude maneuverability of E-sail is restricted if the power supplier of the main spacecraft is bounded. Second, the spin rate increases in the attitude maneuver. Third, both the maneuverability and orbital travel distance increase significantly as the number of main tethers increases. Conversely, they decrease as the initial spin rate and the mass of the remote unit increases. The maneuverability decreases while the orbital travel distance increases when the length of main tether increases.

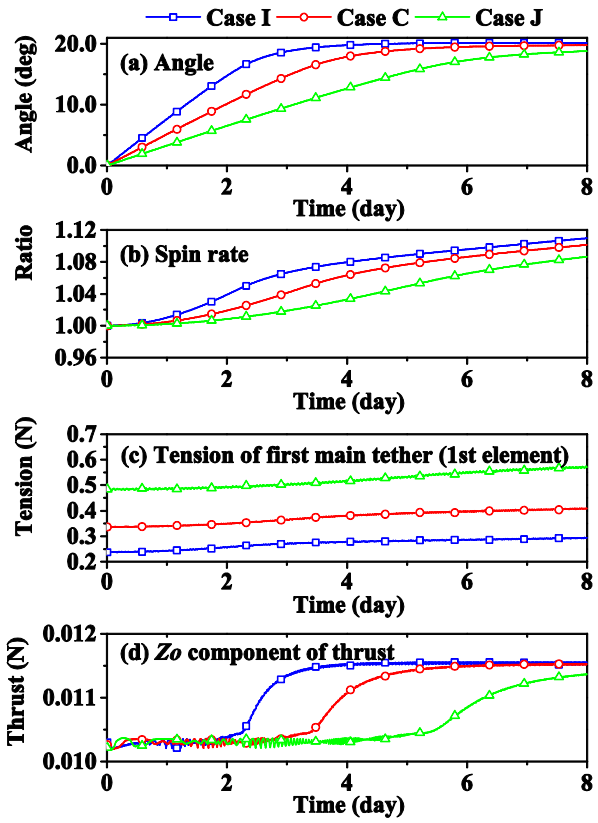

Fig. 14 Influence of remote unit on travel distance, thrust, and dynamic response.

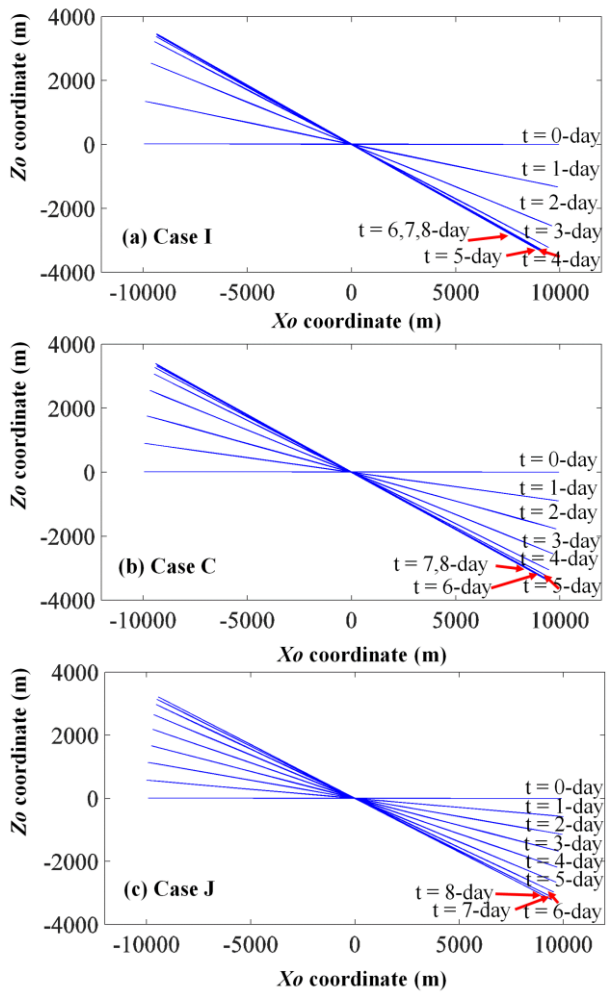

Fig. 15 Influence of remote unit on attitude motion of E-sail.

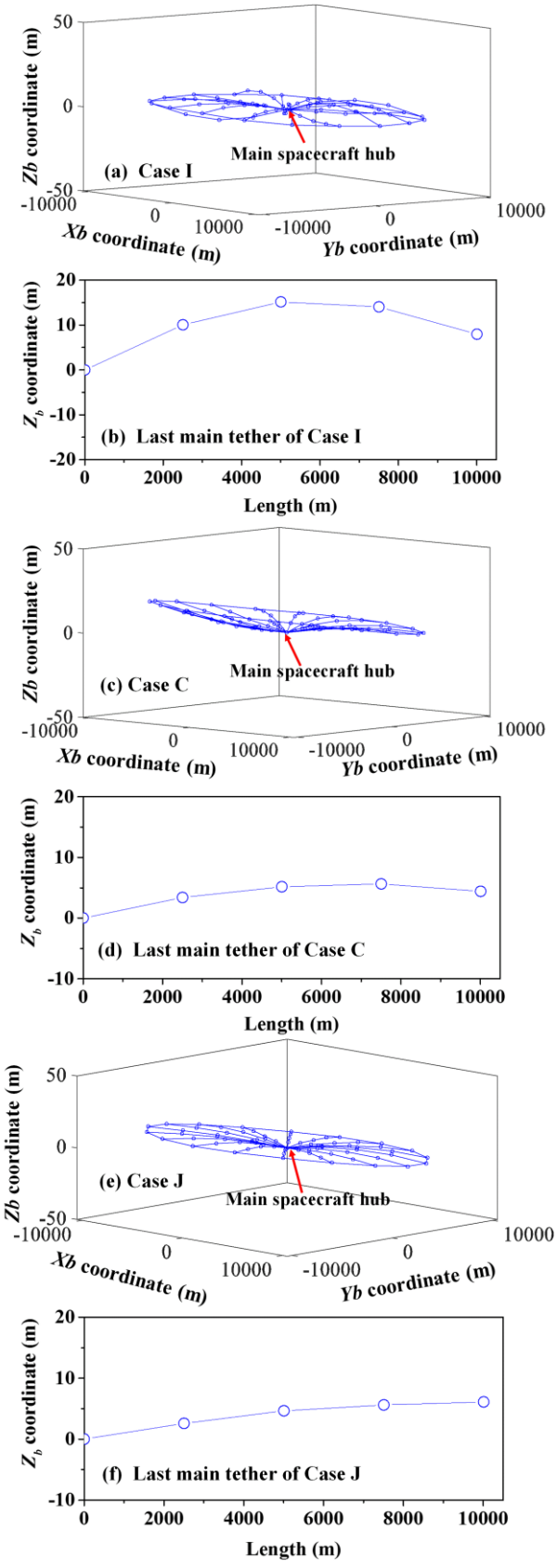
Zb coordinate (m)
50
0
-50
Main spacecraft hub
(a) Case I
-10000
0
10000
Xb coordinate (m)
-10000
0
10000
Yb coordinate (m)
Z_b coordinate (m)
20
10
0
-10
-20
(b) Last main tether of Case I
0
2000
4000
6000
8000
10000
Length (m)
Zb coordinate (m)
50
0
-50
Main spacecraft hub
(c) Case C
-10000
0
10000
Xb coordinate (m)
-10000
0
10000
Yb coordinate (m)
Z_b coordinate (m)
20
10
0
-10
(d) Last main tether of Case C
0
2000
4000
6000
8000
10000
Length (m)
Zb coordinate (m)
50
0
-50
(e) Case J
Main spacecraft hub
-10000
0
10000
Xb coordinate (m)
-10000
0
10000
Yb coordinate (m)
Z_b coordinate (m)
20
10
0
-10
(f) Last main tether of Case J
0
2000
4000
6000
8000
10000
Length (m)

Fig. 16 Influence of remote unit on geometrical configuration of E-sail in body fixed frame (4-day). Left column: (a), (c), (e): 3D view. (b), (d), (f): deflection of main tether.

C. TI concept

The TI type E-sail is proposed to suppress the variation of spin rate in the attitude maneuver, where all (main and auxiliary) tethers are charged and the main tethers are electrically connected to auxiliary tethers at every two main tethers. The advantage of this configuration is that a component of thrust in the spin plane is generated to suppress the increase of spin rate. Before activating the spin rate controller as listed in Eq. (11), the influence of TI type E-sail on the dynamics should be investigated. As listed in Table 5, three cases are analyzed. The physical and controller parameters are the same as those in the case C. The target in-plane and out-of-plane angles (α_t and β_t) are the same as those in the last section.

Table 5 Simulations relate to relative velocity and TI concept effects

Name	Relative Velocity effect	TI effect	Spin rate controller
Case K	Yes	No	No
Case L	No	Yes	No
Case M	Yes	Yes	No
Case N	Yes	Yes	Yes

1. Effect of relative velocity

Here, the effect of the velocity of the solar wind with respect to the tethers on the dynamics of E-sail is investigated. From Table 6 and Fig. 17 (a), the difference is trivial in both the orbital travel distance and in-plane angle due to the slight difference in the thrust force. For example, as listed in Table 6, the attitude maneuver time T_{at} is equal. Thus, it reveals that the effect of the velocity of the solar wind with respect to the tethers has little influence on the attitude maneuverability and orbital motion. On the contrary, a distinct difference in the ratio of spin rate is observed; see Fig. 17(b). Correspondingly, the difference in the tension of the main tether is also distinct. A similar finding of the variation of spin rate was reported in Ref. [25], but the current result is 40% higher in magnitude due to consideration of the effect of relative velocity.

Table 6 Results of relative velocity and TI concept effects

Name	T_t (*day*)	D_{at} (*AU*)
Case C	6.5	6.49×10^{-5}
Case K	6.5	6.43×10^{-5}
Case L	4.4	9.40×10^{-5}
Case M	4.3	9.31×10^{-5}

2. Effect of TI type

The TI type E-sail system is chosen while the effect of velocity of the solar wind with respect to the E-sail is not considered temporarily to show the effect of TI type. The properties of auxiliary tether used in section D are kept the same as the case C except they are electrically conductive. From Table 6 and Fig. 18(c), the TI type E-sail travels more distance because the thrust increases due to more conductive tethers are in effect. Moreover, the TI type E-sail is beneficial to improve the attitude maneuverability. For example, as listed in Table. 6, the attitude maneuver time is 4.4 days shorter than the one of 6.5 days of non-TI type E-sail. The TI type E-sail also helpful for suppressing the increase of spin rate due to the extra thrust component in the spin plane, see in Figs. 18(b) and (c). For example, the spin rate only increases by 6.2% compared with 10% of case C – non-TI type E-sail.

3. Combined effects

Now both the effects of the velocity of the solar wind with respect to the tethers and TI type E-sail are considered. The same properties of auxiliary tethers in section D are used. Regarding the attitude maneuverability in terms of the in-plane angle α, the same conclusion can be obtained by comparing the results of case *L*, see Fig. 18(a) and Fig. 19(a). Moreover, the variation of the orbital travel distance of E-sail under the combined effects is the same as the result of the case *L*. The reason is that the effect of solar wind relative velocity has a negligible effect on the thrust as shown in Fig. 19(c). However, the spin rate is suppressed under the combined effect due to the counterbalance of these two effects. The spin rate increases 8.8 % in the current case, which is less than the results of cases *L* and *M*.

Based on these analyses, it shows the effect of the velocity of solar wind with respect to the E-sail has a considerable influence on the variation of spin rate. Moreover, the TI type E-sail could reduce

the increased amount of spin rate and increase thrust by conductive auxiliary tethers, although the spin rate still increases slightly. Therefore, the control strategy for suppressing the increase of spin rate is still needed.

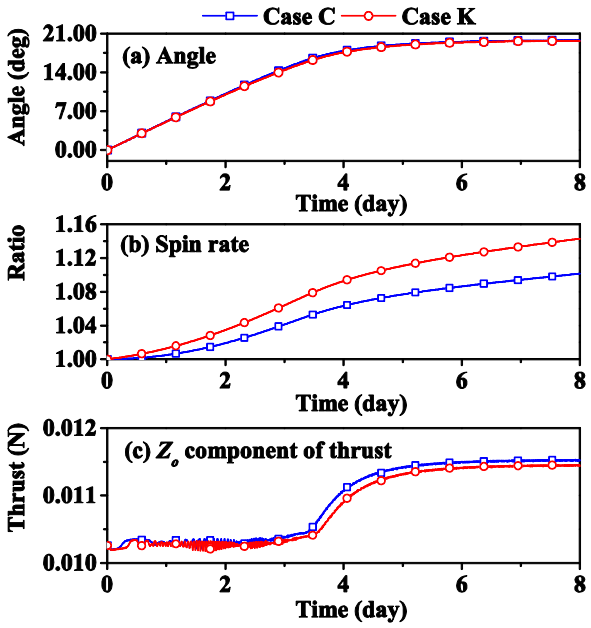

Fig. 17 Comparison of flight dynamics under relative velocity effect.

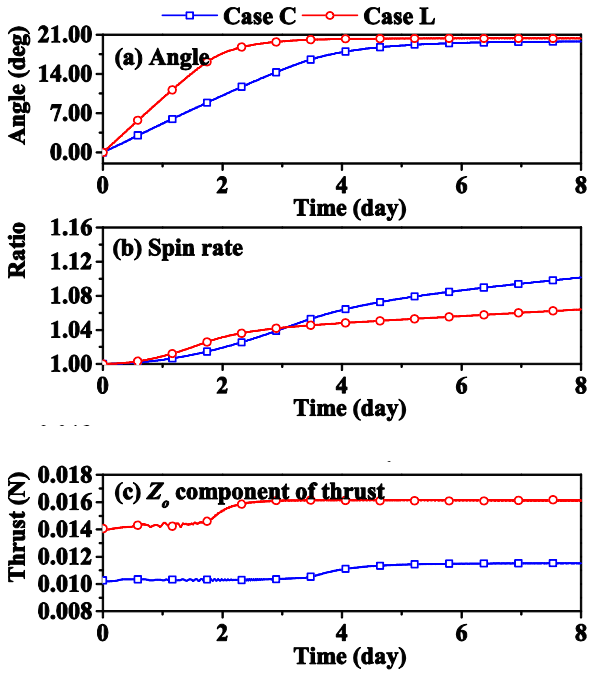

Fig. 18 Comparison of flight dynamics under TI effect.

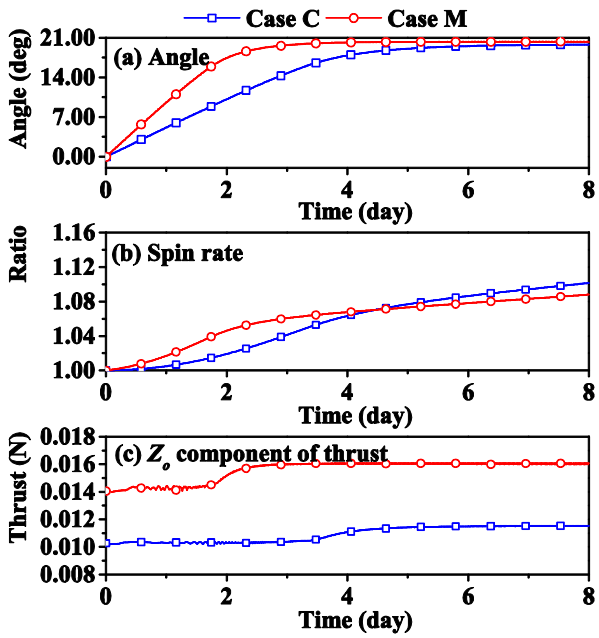

Fig. 19 Comparison of flight dynamics under combined effects.

D. Application of Proposed Spin Rate Control Law

As presented in Section C, the spin rate increases even for the TI type E-sail. In this section, we demonstrate that it can be suppressed by the proposed spin rate controller listing in Eq. (11). The controller gain u_2 of spin rate is set as 50.

As shown in Fig. 20(c), it can be easily found that the proposed spin rate controller works successfully for the TI type E-sail. Moreover, it is seen that the spin rate increases in the attitude-maneuver phase, and then it decreases in the attitude-keeping phase. Different from previous results without the spin rate controller, the in-plane angle α has an overshoot when the spin rate controller is active in the attitude-keeping phase. The phenomenon can be observed from the variation of tether voltage in the first main tether, see Fig. 21. Besides, Figure 20(d) shows the proposed spin rate control has a negligible impact on the thrust and orbital travel distance. Finally, it is concluded that the proposed spin rate control works well based on orbital thrust reduction.

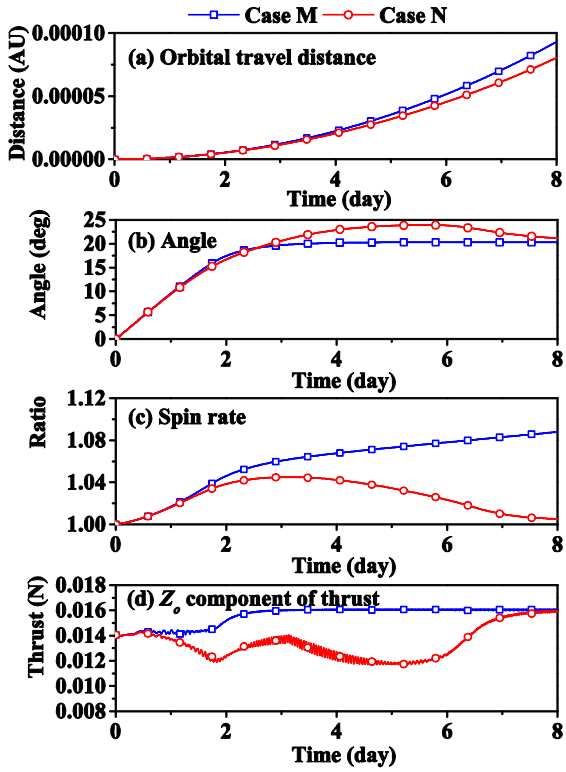

Fig. 20 Comparison of flight dynamics with/without spin rate control

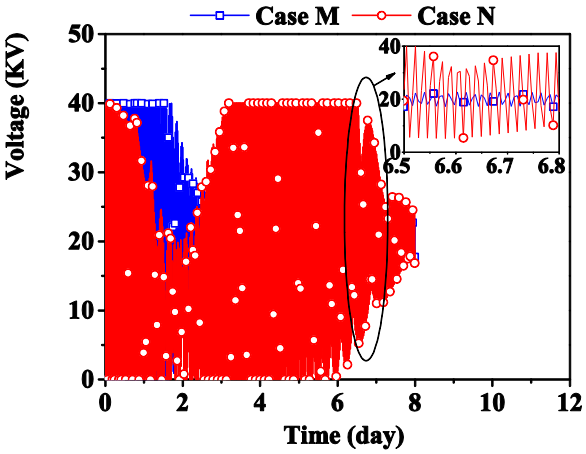

Fig. 21 Voltage modulation of first main tether.

IV. Conclusions

This paper studies the flight dynamics and control strategy of electric solar wind sails with the consideration of coupled elastic and electrical effects. First, an approximate method is proposed to evaluate the spin axis or normal vector of the spin plane. Second, a parametric study is conducted to

investigate the influence of physical parameters, the number of the main tethers, the length of main tether, the initial spin rate, and the mass of remote units, on orbital and attitude dynamic motions. The results show they have a significant impact on the flight dynamics of E-sail when the power of main spacecraft hub is constrained. The maneuverability and orbital travel distance increase significantly when the number of main tethers increases. Conversely, they decrease when the initial spin rate and the mass of the remote unit increases. The maneuverability decreases while the orbital travel distance increases when the length of the main tether increases. Third, the effects of the velocity of the solar wind with respect to the E-sail and the TI type E-sail on the dynamics are investigated. The effect of velocity has a considerable influence on the variation of spin rate, and this effect should be considered. Finally, the spin rate controller works successfully under the TI type E-sail.

Acknowledgements

This work is supported by Discovery Grant (RGPIN-2018-05991) and Discovery Accelerate Supplement Grant (RGPAS-2018-522709) of Natural Sciences and Engineering Research Council of Canada.

References

[1] Janhunen P., "Electric Sail for Spacecraft Propulsion," *Journal of Propulsion and Power*, Vol. 20, No. 4, 2004, pp. 763-764.
doi: 10.2514/1.8580

[2] Janhunen P., Sandroos A., "Simulation study of solar wind push on a charged wire: basis of solar wind electric sail propulsion," *Annales Geophysicae*, Vol. 25, No. 3, 2007, pp. 755-767. doi: 10.5194/angeo-25-755-2007

[3] Mengali G., Quarta A.A., Janhunen P., "Electric Sail Performance Analysis," *Journal of Spacecraft and Rockets*, Vol. 45, No. 1, 2008, pp. 122-129.
doi: 10.2514/1.31769

[4] Huo M., Cao S., Liu Y., Liao H., Qi N., "Mission Analysis for Vesta and Ceres Exploration using Electric Sail with Classical and Advanced Thrust Models," *IEEE Transactions on Aerospace and Electronic Systems*, in press. 2019, pp. 1-16.
doi: 10.1109/TAES.2019.2897040

[5] Mengali G., Quarta A.A., "Non-Keplerian orbits for electric sails," *Celest Mech Dyn Astr*, Vol. 105, No. 1, 2009, pp. 179-195.
doi: 10.1007/s10569-009-9200-y

[6] Quarta A.A., Mengali G., "Electric Sail Mission Analysis for Outer Solar System Exploration," *Journal of Guidance, Control, and Dynamics*, Vol. 33, No. 3, 2010, pp. 740-755.
doi: 10.2514/1.47006

[7] Sanchez-Torres A., "Drag and propulsive forces in electric sails with negative polarity," *Advances in Space Research*, Vol. 57, No. 4, 2016, pp. 1065-1071.
doi: 10.1016/j.asr.2015.12.013

[8] Sanchez-Torres A., "Propulsive Force in an Electric Solar Sail," *Contributions to Plasma Physics*, Vol. 54, No. 3, 2014, pp. 314-319.
doi: 10.1002/ctpp.201410077

[9] Janhunen P., "On the feasibility of a negative polarity electric sail," *Ann. Geophys.*, Vol. 27, No. 4, 2009, pp. 1439-1447.
doi: 10.5194/angeo-27-1439-2009

[10] Janhunen P., Toivanen P., Envall J., Merikallio S., Montesanti G., del Amo J.G., Kvell U., Noorma M., Lätt S., "Overview of electric solar wind sail applications," *Proceedings of the Estonian Academy of Sciences*, Vol. 63, No. 2, 2014, pp. 267-278.
doi: 10.3176/proc.2014.2S.08

[11] Liu C., Tian Q., Yan D., Hu H., "Dynamic analysis of membrane systems undergoing overall motions, large deformations and wrinkles via thin shell elements of ANCF," *Computer Methods in*

Applied Mechanics and Engineering, Vol. 258, No. 2013, pp. 81-95.

doi: 10.1016/j.cma.2013.02.006

[12] Frisbee R.H., "Advanced Space Propulsion for the 21st Century," *Journal of Propulsion and Power*, Vol. 19, No. 6, 2003, pp. 1129-1154.

doi: 10.2514/2.6948

[13] Janhunen P., Quarta A., Mengali G., "Electric solar wind sail mass budget model," *Geoscientific Instrumentation, Methods and Data Systems*, Vol. 2, No. 1, 2013, pp. 85-95.

doi: 10.5194/gi-2-85-2013

[14] Toivanen P., Janhunen P., Envall J., "Electric sail control mode for amplified transverse thrust," *Acta Astronautica*, Vol. 106, January–February, 2015, pp. 111-119.

doi: 10.1016/j.actaastro.2014.10.031

[15] Wie B., "Solar Sail Attitude Control and Dynamics, Part 1," *Journal of Guidance, Control, and Dynamics*, Vol. 27, No. 4, 2004, pp. 526-535.

doi: 10.2514/1.11134

[16] Fu B., Sperber E., Eke F., "Solar sail technology—A state of the art review," *Progress in Aerospace Sciences*, Vol. 86, No. 2016, pp. 1-19.

doi: 10.1016/j.paerosci.2016.07.001

[17] Kun Z., "Control Capability and Allocation of Solar Sail Tip Vanes over Bounded Movement," *Journal of Guidance, Control, and Dynamics*, Vol. 38, No. 7, 2015, pp. 1340-1344.

doi: 10.2514/1.g000938

[18] Wie B., "Solar Sail Attitude Control and Dynamics, Part Two," *Journal of Guidance, Control, and Dynamics*, Vol. 27, No. 4, 2004, pp. 536-544.

doi: 10.2514/1.11133

[19] Fu B., Eke F.O., "Attitude Control Methodology for Large Solar Sails," *Journal of Guidance, Control, and Dynamics*, Vol. 38, No. 4, 2015, pp. 662-670.

doi: 10.2514/1.g000048

[20] Tsuda Y., Saiki T., Funase R., Mimasu Y., "Generalized Attitude Model for Spinning Solar Sail Spacecraft," *Journal of Guidance, Control, and Dynamics*, Vol. 36, No. 4, 2013, pp. 967-974. doi: 10.2514/1.59516

[21] Guerrant D., Lawrence D., "Tactics for Heliogyro Solar Sail Attitude Control via Blade Pitching," *Journal of Guidance, Control, and Dynamics*, Vol. 38, No. 9, 2015, pp. 1785-1799. doi: 10.2514/1.g000861

[22] Li G., Zhu Z.H., Du C., Meguid S.A., "Characteristics of coupled orbital-attitude dynamics of flexible electric solar wind sail," *Acta Astronautica*, Vol. 159, June, No. 2019, pp. 593-608. doi: 10.1016/j.actaastro.2019.02.009

[23] Toivanen P., Janhunen P., Envall J., Merikallio S., "Electric solar wind sail control and navigation," Advances in the Astronautical Sciences, Vol, 145, 2012, pp. 275-285.

[24] Toivanen P.K., Janhunen P., "Spin Plane Control and Thrust Vectoring of Electric Solar Wind Sail," *Journal of Propulsion and Power*, Vol. 29, No. 1, 2012, pp. 178-185. doi: 10.2514/1.B34330

[25] Janhunen P., Toivanen P., "TI tether rig for solving secular spinrate change problem of electric sail," *arXiv preprint arXiv:1603.05563*, May, 2017.

[26] Janhunen P., Toivanen P., "An intrinsic way to control E-sail spin," *arXiv preprint arXiv:1406.6847*, June, 2014.

[27] Janhunen P., "Photonic spin control for solar wind electric sail," *Acta Astronautica*, Vol. 83 February–March, 2013, pp. 85-90. doi: 10.1016/j.actaastro.2012.10.017

[28] Janhunen P., Toivanen P., Polkko J., Merikallio S., Salminen P., Haeggström E., Seppänen H., Kurppa R., Ukkonen J., Kiprich S., "Electric Solar Wind Sail In-Space Propulsion Status Report," *Proceedings of Space Propulsion,* European Space Agency, 2010.

[29] Bassetto M., Mengali G., Quarta A.A., "Attitude dynamics of an electric sail model with a realistic shape," *Acta Astronautica*, Vol. 159, June, 2019, pp. 250-257.
doi: 10.1016/j.actaastro.2019.03.064

[30] Janhunen P., "Electric sail, photonic sail and deorbiting applications of the freely guided photonic blade," *Acta Astronautica*, Vol. 93, January, 2014, pp. 410-417.
doi: 10.1016/j.actaastro.2013.07.041

[31] Montalvo C., Wiegmann B., "Electric sail space flight dynamics and controls," *Acta Astronautica*, July, 148 No. 2018, pp. 268-275.
doi: 10.1016/j.actaastro.2018.05.009

[32] Liu F., Hu Q., Liu Y., "Attitude Dynamics of Electric Sail from Multibody Perspective," *Journal of Guidance, Control, and Dynamics*, Vol. 41, No. 12, 2018, pp. 2633-2646.
doi: 10.2514/1.g003625

[33] Bassetto M., Mengali G., Quarta A.A., "Stability and Control of Spinning Electric Solar Wind Sail in Heliostationary Orbit," *Journal of Guidance, Control, and Dynamics*, Vol. 42, No. 2, 2019, pp. 425-431.
doi: 10.2514/1.g003788

[34] Li G.Q., Zhu Z.H., "Long-term dynamic modeling of tethered spacecraft using nodal position finite element method and symplectic integration," *Celest Mech Dyn Astr*, Vol. 123, No. 4, 2015, pp. 363–386.
doi: 10.1007/s10569-015-9640-5

[35] Li G., Zhu Z.H., Cain J., Newland F., Czekanski A., "Libration Control of Bare Electrodynamic Tethers Considering Elastic–Thermal–Electrical Coupling," *Journal of Guidance, Control, and Dynamics*, Vol. 39, No. 3, 2015, pp.642-654.
doi: 10.2514/1.G001338

[36] Sun F., Zhu Z., LaRosa M., "Dynamic modeling of cable towed body using nodal position finite

element method," *Ocean Engineering*, Vol. 38, No. 4, 2011, pp. 529-540.
doi: 10.1016/j.oceaneng.2010.11.016.

[37] Li G., Zhu Z.H., "Precise Analysis of Deorbiting by Electrodynamic Tethers Using Coupled Multiphysics Finite Elements," *Journal of Guidance, Control, and Dynamics*, Vol. 40, No. 12, 2017, pp. 3348-3357.
doi: 10.2514/1.g002738